JACS Au
AN OPEN ACCESS JOURNAL OF THE AMERICAN CHEMICAL SOCIETY

pubs.acs.org/jacsau

Article

Controlled Synthesis of Metal–Organic Frameworks in Scalable Open-Porous Contactor for Maximizing Carbon Capture Efficiency

Young Hun Lee, YongSung Kwon, Chaehoon Kim, Young-Eun Hwang, Minkee Choi, YouIn Park, Aqil Jamal, and Dong-Yeun Koh*

Cite This: *JACS Au* 2021, 1, 1198–1207

Read Online

ACCESS | Metrics & More | Article Recommendations | Supporting Information

ABSTRACT: Metal–organic frameworks (MOFs) are a class of microporous materials that have been highlighted with fast and selective sorption of gas molecules; however, they are at least partially unstable in the scale-up process. Here, we report a rational shaping of MOFs in a scalable architecture of fiber sorbent. The long-standing stability challenge of MOFs was resolved by using stable metal oxide precursors that are subject to controlled surface oxide dissolution-growth chemistry during the Mg-based MOF synthesis. Highly uniform MOF crystals are synthesized along with the open-porous fiber sorbents networks, showing unprecedented cyclic CO_2 capacities in both flue gas and direct air capture (DAC) conditions. The same chemistry enables an in situ flow synthesis of Mg-MOF fiber sorbents, providing a scalable pathway for MOF synthesis in an inert condition with minimal handling steps. This modular approach can serve both as a reaction stage for enhanced MOF fiber sorbent synthesis and as a "process-ready" separation device.

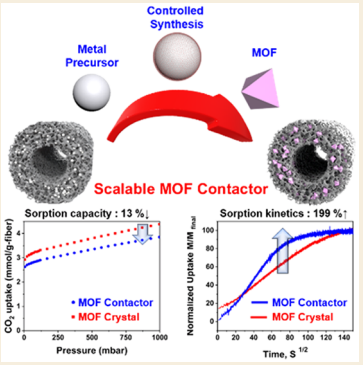

KEYWORDS: *metal–organic frameworks, fiber sorbents, controlled-dissolution synthesis, postspinning conversion, amine functionalization, carbon capture and storage*

1. INTRODUCTION

Future energy systems will still rely on the combustion of hydrocarbons, which generates electricity at the cost of emitting carbon dioxide into the atmosphere.[1,2] Though prevailing technologies for carbon capture and storage (CCS) such as wet amine scrubbing have the potential for high rates of recovery of CO_2, they are energy-intensive, which requires more than 30% of the parasitic energy load of the power plant.[3,4] The CCS energy efficiency could be improved if paired with low-energy porous solid-based separations that effectively capture and release CO_2 from diverse flue gas streams. Numerous porous solids, including amine-functionalized silica[5,6] and metal–organic frameworks (MOFs), have been widespread solutions for CO_2 capture on a lab scale.[7−9] However, they have not been broadly demonstrated in realistic conditions because of the relative scarcity of the microporous materials that are integrated into a scalable fluid contactor that permits low pressure drop, large sorption capacity, fast kinetics, and regeneration stability. Fiber sorbents provide the best combination of these four metrics, but to date, they have not been sufficiently effective for integrating high-performance porous solids such as MOFs.[10]

The insertion of alkylamines to open-metal sites within the pores of metal–organic frameworks with expanded lattices has been an effective strategy to enhance CO_2 sorption capacity at low partial pressures and stability under humid conditions.[11,12] For instance, Mg_2(dobpdc) (dobpdc^{4-} = 4,4′-dioxidobiphenyl-3,3′-dicarboxylate) tethered with either diamines or tetraamines is one of the most highlighted porous materials that have exhibited exceptional capacity and stability.[13,14] These MOFs feature a cooperative CO_2 capture mechanism achieved by continuous deprotonation and nucleophilic reactions between adjacent amine groups that rapidly create an ammonium carbamate chain reaction, thus enabling large CO_2 uptake even at low partial pressures.[13] Due to their steplike sorption behavior, these MOFs have a large CO_2 swing capacity and nearly perfect desorption during the temperature swing adsorption process.[15] Recently, the insertion of a tetraamine, namely, *N*,*N*′-bis(3-aminopropyl)-1,4-diaminobutane, into the pores of the Mg_2(dobpdc) was demonstrated with exceptional stability upon steam regeneration since the bulky tetraamine group strongly coordinates onto the metal sites in MOF.[14] In diamine-Mg_2(dobpdc), one diamine molecule is attached to one open-metal site in the MOF. On the other hand, one tetraamine molecule is bound to two open-metal sites in tetraamine-Mg_2(dobpdc) (Figure S1). This unique coordination and the use of less volatile tetraamine groups made it possible to increase the lifespan of the amine-

Received: February 16, 2021
Published: June 21, 2021

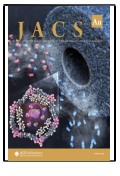

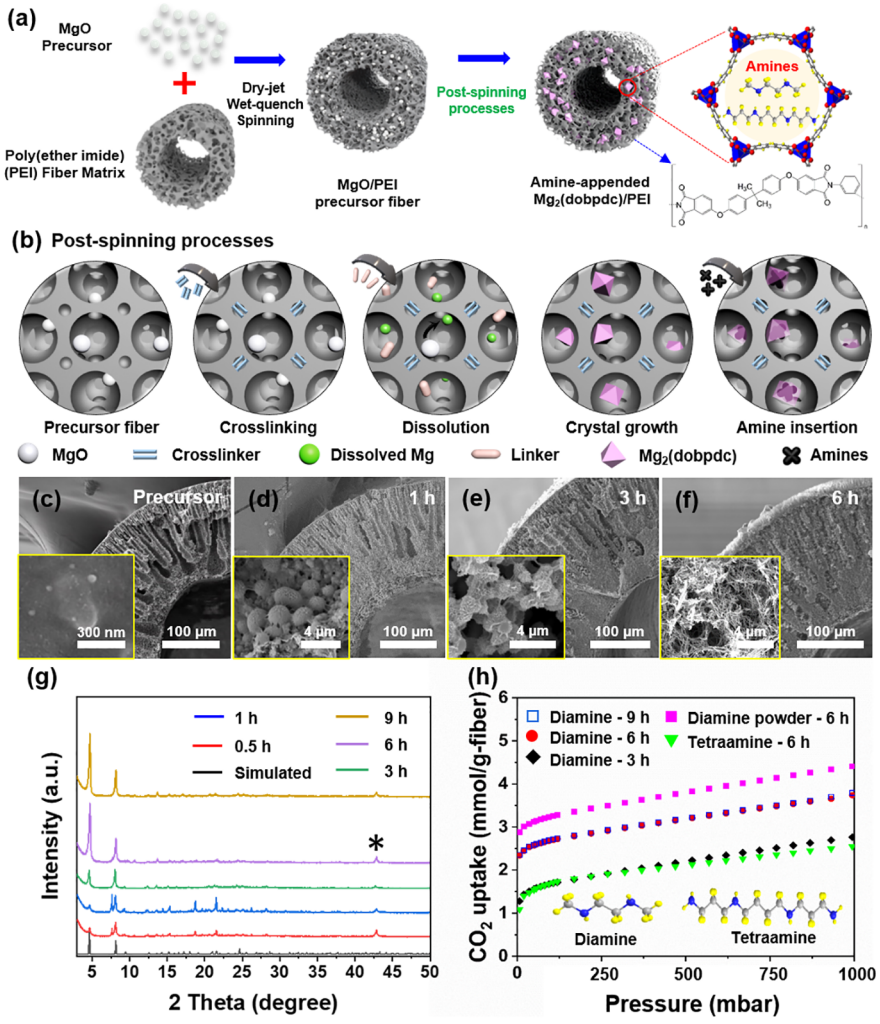

Figure 1. (a,b) Scheme of the synthetic route of amine functionalized-Mg_2(dobpdc)/PEI fiber sorbents. To bypass the aqueous fiber spinning (but highly scalable) process with MOF crystals, precursor fibers with water-stable metal oxide precursors are produced. As-spun fibers are cross-linked, and metal oxide conversion into ultramicroporous frameworks is subsequently performed. Finally, amine moieties are infused into the MOF to further drive up the CO_2 capacity and humidity stability of the fiber sorbents. (c–f and inset) SEM cross-sectional images for the MgO/PEI precursor fibers with 46 wt % of 50 nm MgO and Mg_2(dobpdc)/PEI fiber sorbents obtained according to MOF conversion times. (g) XRD diffractions of the Mg_2(dobpdc)/PEI fiber sorbents synthesized at various reaction times. Asterisk (*) indicates the peak of unreacted MgO. (h) Dry CO_2 uptake of the diamine-Mg_2(dobpdc) powder and the diamine-/tetraamine-Mg_2(dobpdc)/PEI fiber sorbents from Mg_2(dobpdc)/PEI fiber sorbents obtained by various reaction times under 25 °C and 1 bar. Carbon (gray circle), nitrogen (blue circle), hydrogen (yellow circle), oxygen (red circle), and magnesium (blue tetrahedron) in material structures.

functionalized MOFs in practical conditions. Nevertheless, there is a gap between the lab and industry, which is only solvable by integrating these microporous materials into the scalable shapes that can fit into appropriate industrial separation devices. The fiber sorbent architecture provides a symmetrically open-porous polymer matrix with a homogeneously dispersed sorbent phase, usually up to 75–80 wt % sorbent loading. This unique structure reduces the average diffusion length of adsorbates compared to an inorganic monolith, ultimately resulting in improved separation efficiency (Figure S2).[10,16] Scaled up synthesis of the fiber sorbents is achieved via the dry-wet spinning technique using water as a quench medium, making industrial-scale production possible. Sorbents such as zeolites and amine-impregnated silica with excellent water, chemical, and thermal and mechanical stabilities allow direct fiberspinning, and we shall refer to these fiber sorbents as Type 1 fiber sorbents.[17,18] On the other hand, some MOF classes with open-metal sites that are unstable in water cannot be processed in spinning process.[16] Amine tethering onto the open-metal sites enhances the water stability but is limited to humid CO_2 capture conditions. The high-shear mixing and water quenching in the fiber spinning process exert severe mechanical stress to amine moieties.[19] Instead of directly incorporating microporous materials into the fiber, the water-stable and mechanically rigid metal oxide precursor loaded fibers can be fabricated. Then the precursor-loaded fibers are converted into MOF fiber sorbents in the Type 2 route.

Here, we investigate the controlled synthesis of Mg-based MOF nanocrystals within a polymeric fiber loaded with stable metal oxide precursors using the Type 2 route. A scalable MOF synthesis approach has been developed, where Mg^{2+} ions are etched from the surface oxide and are incorporated into the MOF structure, enabling regulated growth of MOF nanocryst-

https://doi.org/10.1021/jacsau.1c00068
JACS Au 2021, 1, 1198–1207

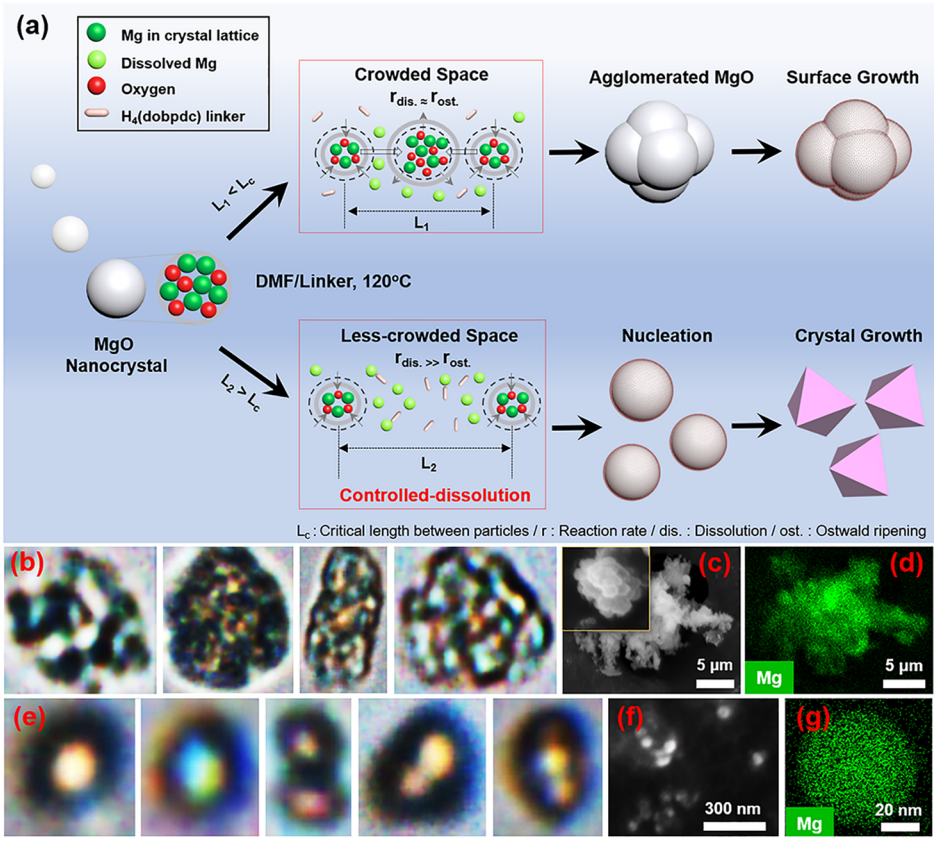

Figure 2. (a) Cartoon illustrating the MOF conversion process from a MgO nanocrystal within the confined spaces. L_c refers to the critical length between particles in which MgO recrystallization does not occur due to Ostwald ripening. (b) Digital images of MgO crystals obtained after 30 min of MOF conversion from MgO/PEI fiber precursors loaded at 71 wt % (high-loading) through a fluid imaging apparatus (FlowCam) and corresponding SEM and EDS mapping of the MgO crystals (c,d). (e) Digital images of MgO crystals obtained after 30 min of MOF conversion from MgO/PEI fiber precursors loaded at 46 wt % (low-loading) through a fluid imaging apparatus (FlowCam) and corresponding SEM and EDS mapping of the MgO crystals (f,g).

als.[20] A mild removal of the Mg^{2+} ions from the surface layers in a less-crowded pore space allowed a systematic and controlled dissolution-growth of MOF nanocrystals. We demonstrate the utility of this chemistry via in situ flow synthesis in a module packaged with precursor fibers, showing that the scalable production of MOF fiber sorbents is possible. The amine-appended Mg_2(dobpdc) fiber sorbents discussed in this work selectively capture CO_2 with productivities over 4 mmol per gram of the fiber, under humid flue gas conditions, at least five times higher than those of state-of-the-art amine-functionalized silica-based fiber sorbents.[21]

2. RESULTS AND DISCUSSION

2.1. Control of MOF Growth in Fiber Sorbents

Figure 1a and b shows the synthesis route for MOF fiber sorbents in this work. Syringe tests produced small-scale fiber sorbent precursors (<10 cm in length) for the initial assessment of the fiber morphology and characterization of the materials before the full-scale fiber spinning (>100 m in total length). We investigated various dope solution compositions using MgO nanoparticles as seeds for MOF growth and poly(ether imide) (PEI) as a mesoporous polymeric support (Table S1). In an ideal fiber sorbent, nano- to microsized sorbent particles should be dispersed throughout the open-porous polymer matrix to minimize diffusion resistance so that the uptake equilibration time can be decreased, which further translates into the capability to build more productive, smaller separation devices.[22] The effect of incorporating MgO nanoparticles with different loadings (25–73 wt %) and particle sizes (50 and 300 nm) on the open-porous structure of the polymeric matrix was assessed. The dry weight loading of MgO of the formed MgO/PEI precursor fiber was calculated via thermogravimetric analysis (TGA) (Figure S3). As shown in Table S1, when the MgO content in the dope solution was approximately four times higher than that of the polymer, the maximum dry MgO loading of 73 wt % was achieved. A MgO loading over 73 wt % was deemed impractical because of the extremely high viscosity of the resultant solution, which hampers the solution processing via spinning technology.[23] As shown in the cross-sectional scanning electron microscopy (SEM) images and energy-dispersive X-ray spectroscopy (EDS) pattern of the formed fibers (Figures S4 and S5), open-porous structures with some macrovoids were obtained in all fibers except for the 73 wt % fiber. Additionally, minimal leaching of MgO nanoparticles (both 50 and 300 nm) during the syringe test indicates that stable, large-scale spinning is possible (Table S1). The long-chain linker of 4,4′-dihydroxy-(1,1′-biphenyl)-3,3′-dicarboxylic acid (Figure S6) is only soluble in aprotic solvents such as dimethylformamide (DMF). Therefore, to proceed with further MOF synthesis within the fiber, reinforcement in chemical and physical stability of the poly(ether imide) was essential.[24] Both thermal (i.e., heat treatment at 300 °C) and

https://doi.org/10.1021/jacsau.1c00068
JACS Au 2021, 1, 1198–1207

chemical (i.e., ethylenediamine and *p*-xylylenediamine assisted) cross-linking was performed using the as-spun small-scale precursor fibers. The cross-linked precursor fibers were then converted into a Mg_2(dobpdc)/poly(ether imide) fiber sorbent (hereafter, Mg_2(dobpdc)/PEI) to elucidate the effect of cross-linking on MOF conversion. As shown in Figure S7a, the MOF conversion was low in the thermally cross-linked fiber indicated by the peak at 44° of unreacted MgO remaining in the matrix,[25] reflecting the kinetically limited diffusion of linker molecules in thermally shrunk fibers. On the other hand, chemically cross-linked precursor fibers showed nearly complete MOF conversion without damage to the fiber matrix (Figure S7b). Subsequently, MOF growth was optimized on the chemically cross-linked MgO/PEI precursor fibers by changing the molar concentration of the ligand solution, reaction temperature, and time. Figure S8a shows XRD patterns of the Mg_2(dobpdc)/PEI synthesized using the different molar concentrations of the linker from 0.19 to 0.29 M. The higher the ligand concentration, the higher the MgO etching rate, which promoted the MOF growth;[20] however, when it exceeded 0.26 M, unreacted ligands showed up in the XRD pattern and these ligands recrystallized on the surface of the fiber (Figure S9). Similarly, the MOF crystallization rate was accelerated at high temperature, resulting in near-complete MOF conversion at 120 °C (Figure S8b). Figure 1c−g shows SEM cross sections and XRD patterns of MOF fiber sorbents from MgO/PEI precursor fibers by controlling synthesis times at fixed reaction conditions of 0.26 M and 120 °C. Spherical MgO precursors are converted into the rod-shaped Mg_2(dobpdc) as the reaction proceeds. The inset images in Figure 1c−f show a series of transformations from MgO to Mg_2(dobpdc). Within the first hour of the MOF conversion, Mg^{2+} ions etched out from the MgO are nucleated into Mg_2(dobpdc) across the MgO surfaces (Figure 1d and g). The degree of MgO surface etching and the growth of MOF clusters are accelerated up to 3 h of reaction, resulting in particles with urchin-like morphologies (Figure 1e). At 6 h, needle-shaped Mg_2(dobpdc) crystals were fully grown along the 1D direction due to the anisotropic crystal structure (Figure 1f and g). The fiber samples were collected with different reaction times, and they were subjected to X-ray diffraction to determine the rate of MgO conversion to Mg_2(dobpdc). As shown in Figure 1g, no significant change was observed after 6 h of reaction. The relative intensity ratio between the (100) peak of Mg_2(dobpdc) at 4.8° and the unreacted MgO at 42.8° increased to ∼85 000:1, after 6 h of reaction, which indicates that most of the MgO were converted into Mg_2(dobpdc). (Figures 1g and S10a−c). Furthermore, it was challenging to maintain the original morphology and the mechanical strength of the fiber sorbents over 9 h of reaction due to the prolonged attack of the aprotic reaction mixture on the polymer phase (Figure S10d). SEM images and EDS of the optimal Mg_2(dobpdc)/PEI fiber sorbents synthesized at 6 h demonstrated that the porous structure of the fiber was well maintained with the homogeneous MOF conversion (Figure S11). Thus, diamine and tetraamine are inserted into the optimized MOF fiber sorbents via a solvent-assisted impregnation method in batch reactors, and then the CO_2 sorption capacity of the samples under 25 °C at 1 bar (Figure 1h) is tested.

When MOFs are converted from MgO precursors in a fiber matrix, the dissolution step of MgO is essential because this step determines the MOF conversion time scale and the overall architecture of the fiber. An illustration explaining the controlled dissolution of MgO nanoparticles within the confined pore space is shown in Figure 2a. The synthetic approach breaks down to (i) dissolution on the surface of metal oxide, (ii) diffusion of metal ions and ligands, (iii) MOF nucleation and growth, and (iv) Ostwald ripening between MgO, where the reaction rates at each stage are competitive.[26] The metal oxides serve as a source for Mg^{2+}. The mild synthesis solution with the linker controllably etches the MgO nanoparticles, and as the dissolution of Mg^{2+} progresses, the MOF nucleation occurs with the supplied linker molecules. However, if the surface etching of Mg^{2+} occurs in a highly crowded pore space, with interparticle length below the critical length scale, partial aggregation between adjacent MgO particles is pronounced due to the Ostwald ripening.[27] It is observed that when the MgO nanocrystals are subjected to solvothermal synthesis condition for less than 30 min, the dissolution of the MgO proceeds; however, not enough MOF crystals are nucleated or grown (Figure S16e). Within the first 30 min of MOF conversion, highly crowded fiber precursors (e.g., >71 wt % loading of MgO) showed immediate Ostwald ripening between MgO nanoparticles that leads to the formation of partially converted MOF crystals (Figure 2b−d).

This has resulted in the formation of densified MgO due to the accelerated MgO agglomeration (Figures 2a and S12d−f) in fibers with MgO loading over 46 wt %. For high loadings (>46 wt %), MOF growth occurred on the surface of the densified MgO layer or as a separate layer; therefore, the MOF conversion rate was reduced as the loading MgO increased under the same synthetic conditions (Figures S12d−f, S13, and S14). The effect of the critical interparticle length scale was more pronounced when the large-sized metal oxides (300 nm) were used. Due to the formation of highly dense MgO layers in the crowded pore space, the resultant Mg_2(dobpdc)/PEI did not maintain the original open-porous structure, and severe delamination of the MOF from the polymer layer was observed (Figures S12d−f and S15a−h).

For the controlled dissolution and subsequent MOF growth within the confined pore structures, the MgO loading was suppressed below 50 wt % in the precursor fiber. In this case, interparticle length exceeds the critical length scale, facilitating the MOF growth and minimizing the Ostwald ripening bewteen MgO nanoparticles. In the presence of the organic linker, the kinetics of MgO layer dissolution is coupled to MOF nanocrystal growth, resulting in the formation of uniform Mg-based MOF nanocrystals throughout the polymeric matrix (Figure 2a,e−g and S12a−c). Therefore, Mg_2(dobpdc)/PEI synthesized with the 46 wt % precursor fibers with 50 nm MgO maintained the original open-porous morphology of the polymeric matrix with nearly complete MOF conversion (Figures S13 and S15i−l). This synthetic approach represents an opportunity to reduce the MOF synthesis time (Figures 1g,h and S16) and also provides a method for the highly controlled synthesis of MOF nanocrystals within the confined space. The dry CO_2 isotherms of the diamine (*N*,*N*′-dimethylethylenediamine) and tetraamine (*N*,*N*′-bis(3-aminopropyl)-1,4-diaminobutane) inserted Mg_2(dobpdc)/PEI confirmed the successful synthesis of MOF nanocrystals in the fiber sorbent (Figure 1h). Even though the Mg_2(dobpdc)/PEI from a 46 wt % precursor fiber using 50 nm MgO particles showed a slight loss in CO_2 sorption capacity compared to highly loaded cases (Figure

https://doi.org/10.1021/jacsau.1c00068
JACS Au 2021, 1, 1198−1207

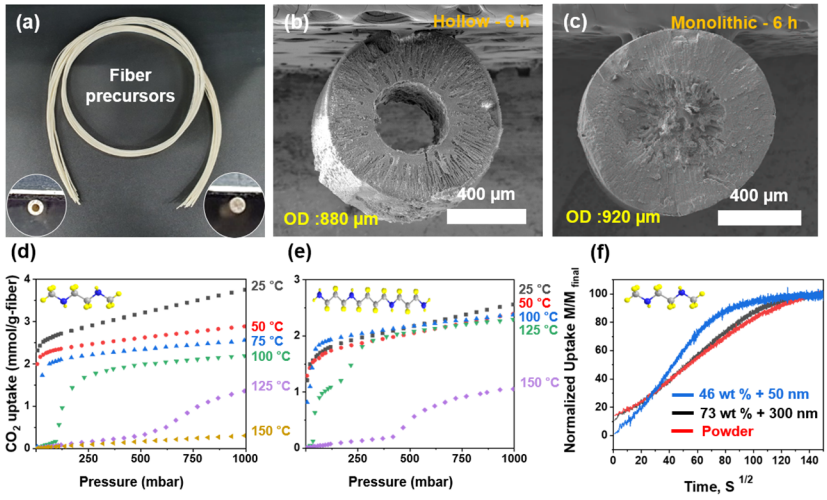

Figure 3. (a) Pictures showing the 50 m bundle of MgO/PEI precursor fibers with 46 wt % loading of 50 nm MgO. The insets present the precursor fibers with hollow (left) and monolithic structure (right). (b,c) Cross-sectional SEM images of the optimized Mg_2(dobpdc)/PEI with (b) hollow and (c) monolithic structures. (d,e) 100% dry CO_2 isotherms of the (d) diamine-Mg_2(dobpdc)/PEI and (e) tetraamine-Mg_2(dobpdc)/PEI under various operating temperatures and 1 bar. (f) Comparisons of normalized CO_2 uptake (M/M_{final} versus square root of time) for diamine-Mg_2(dobpdc) powder (red), diamine-Mg_2(dobpdc)/PEI fiber sorbents from MgO precursor fibers loaded by 46 wt % of 50 nm MgO (blue), and 73 wt % of 300 nm MgO (black) at 60 °C and 1 bar (15% CO_2/85% N_2).

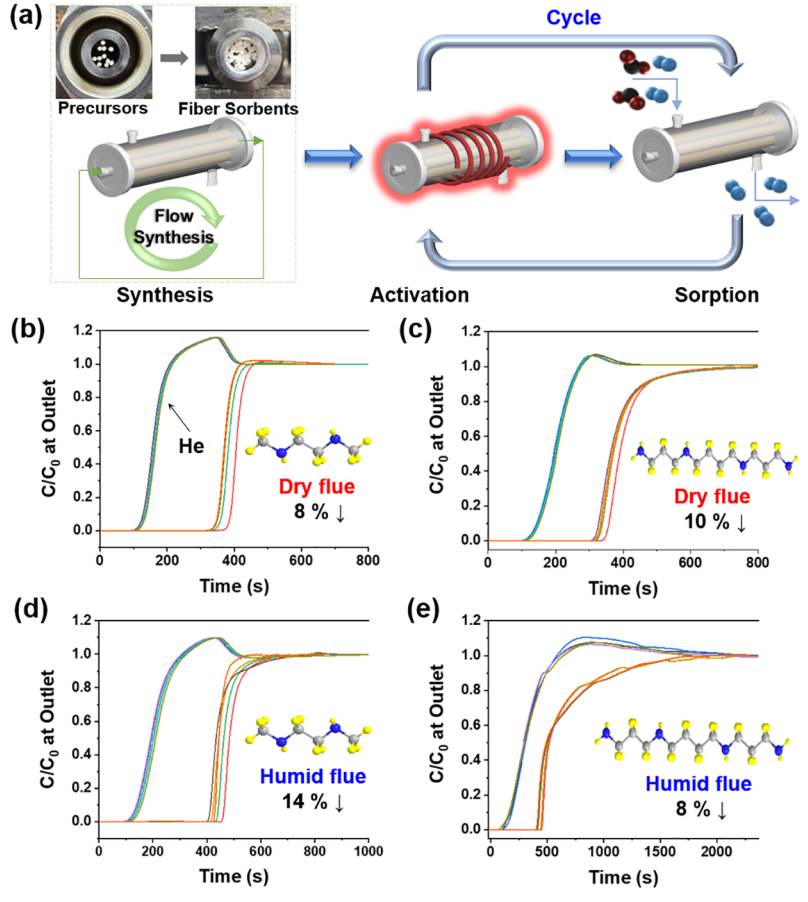

Figure 4. (a) Scheme describing the operating procedures (flow reaction, activation, and cyclic sorption) in the module system. The insets show modules packaged with MgO/PEI precursor fibers (left) and the corresponding amine-appended Mg_2(dobpdc)/PEI (right). (b−e) Cyclic sorption performance of the diamine-/tetraamine-Mg_2(dobpdc)/PEI module (with 11 fibers) via the breakthrough setup at 15% CO_2 and 35 °C under (b,c) dry conditions (adsorption: 15% CO_2, 15% He, in N_2 balance at 35 °C for 10 min; desorption: Ar at 120 °C for 30 min) and (d,e) humid conditions (prehumidification: N_2 100%, RH 100% Ar at 35 °C and 1 bar under 200 sccm for 30 min; adsorption: 15% CO_2, 15% He, RH 100%, in N_2 balance at 35 °C under 30 sccm for 15 min; desorption: Ar at 120 °C for 30 min).

https://doi.org/10.1021/jacsau.1c00068
JACS Au 2021, 1, 1198−1207

S17−19), this fiber had excellent porous morphology for enhanced mass transfer and material processability for large-scale module fabrication.

2.2. Full-Scale MOF Fiber Sorbent

Full-scale precursor fiber spinning was performed with a custom dry-jet wet-quench spinning apparatus (Figure S20 and Table S2) that produces fibers at 10−20 m/min. Figure 3a shows the 50 m MgO/PEI precursor fiber bundle fabricated in this work. With these full-scale precursor fibers, we performed MOF conversion in two different reactor setups to systematically understand the scaling-up process of MOF fiber sorbents: (1) batch synthesis and (2) in situ flow synthesis (Figure S21) for scalable MOF conversion. The precursor fibers had excellent flexibility, but for MOF converted fibers only a slight bend was allowed before destruction because the pores in the polymeric matrix were filled with MOF particles. Mg_2(dobpdc)/PEI synthesized from the batch reactors also had excellent porous structures (Figure 3b and c). The Mg_2(dobpdc)/PEI with a hollow and monolithic structure showed a slight increment in the outer diameter from 607 to 880 μm and from 650 to 920 μm, respectively, after MOF conversion from MgO/PEI precursor fibers. Batch-synthesized Mg_2(dobpdc)/PEI was further functionalized with diamine and tetraamine moieties in the same batch reactor setup. Figure 3d and e shows the dry CO_2 isotherms for diamine- and tetraamine-Mg_2(dobpdc)/PEI under different operating temperatures from 25 to 150 °C. Steplike sorption behavior (Figure S22) was also confirmed in the amine-appended MOF fiber sorbents, which corresponds to the cooperative CO_2 capture mechanism that translated into a high sorption capacity at low CO_2 partial pressures. Different working capacities over specific temperature ranges (i.e., 25−100, 25−125, 25−150 °C) and pressure (i.e., 150 and 1013 mbar) are shown in Table S3. The isosteric heats of sorption (Figure S23) calculated from the isotherms also validate the chemisorptive nature ($-Q_{st}$ = 71 kJ/mol in diamine MOF fiber sorbents and 66−100 kJ/mol in tetraamine MOF fiber sorbents) of the CO_2 sorption process in amine-appended MOF fiber sorbents.[13,14]

The sorption kinetics (Figure 3f) of the MOF fiber sorbents were measured in a pressure-decay sorption apparatus using coal flue gas composition (15 mol % CO_2 and balance N_2) at 1 bar. For the diamine-Mg_2(dobpdc)/PEI, the time to reach the complete equilibrium was shorter than that of the MOF powder case due to the enhanced bulk mass transfer by the open-porous matrix of the MOF fiber sorbents. The mercury porosimetry (Figure S24) showed only a slight reduction of macroporosity in Mg_2(dobpdc)/PEI than that of the precursor fiber, suggesting that the cross-linking of the polymeric matrix effectively enhanced the chemical stability of the fiber while maintaining the overall porosity. Interestingly, the Mg_2(dobpdc)/PEI fabricated from the highly loaded precursor (73 wt %) exhibited a drastically decreased pore volume in the macropore range (0.1−1 μm), which verified that the densification of MgO deteriorated the gas transport of the resultant MOF fiber sorbents (Figures 3f and S24). Amine-appended Mg_2(dobpdc)/PEI fabricated from 46 wt % precursor fiber with 50 nm MgO had a reduced BET surface area (up to 90%) after amine functionalization, indicating the effective insertion of amine groups into the micropores of MOF within the fiber sorbent (Figure S25).

On top of these, we demonstrated the in situ flow synthesis of MOF fiber sorbents in a modular device (Figure 4a). Initially, MgO/PEI precursor fibers were packaged in a 1/4" stainless-steel module, which simultaneously served as a reactor for flow synthesis of MOF fiber sorbent, including polymer cross-linking and amine insertion steps, and a separation device that could be directly used for cyclic CO_2 sorption upon activation. The single-module approach minimizes the handling steps in the synthesis of porous materials as well as in making the separation device. Further, it prevents the MOF fiber sorbents from being directly exposed to moist air or another unwanted atmosphere during the fabrication/synthesis/testing process. Pimentel et al. originally demonstrated a similar approach with ZnO loaded fibers to fabricate HKUST-1 or with ZIF-8 loaded fiber sorbents using relatively benign solvents such as ethanol and water.[28] Figure 4a shows the module used in this study, which depicts how the monolithic MgO/PEI precursor fibers are loaded in the module and further converted to amine-appended MOF fiber sorbents. Flow reaction used in cross-linking, MOF synthesis, and amine insertion could maximize the reaction extent at each step and reduce the overall synthesis cost by recycling the unreacted ligands and solvents.[29] Especially, the flow synthesized fibers showed a higher degree of cross-linking than the batch synthesized fibers as probed by Fourier-transform infrared (FT-IR) spectroscopy and elemental analysis (Figure S26 and Table S4), which was advantageous in producing a more mechanically stable MOF fiber sorbent. With the optimized flow synthesis protocols (see Syntheses in the Supporting Information), modules containing multiple strands of diamine- and tetraamine-Mg_2(dobpdc)/PEI were fabricated and tested in a custom-built breakthrough system (Figure S27).

2.3. CO_2 Sorption at Flue Gas Compositions

Figure S28 compares the pressure drop as a function of superficial velocity for modules containing different amounts of diamine-Mg_2(dobpdc)/PEI fibers, which is a critical design factor in the fluid contactor showing the ability to process high gas flow rates. The void fraction and corresponding dry CO_2 breakthrough curves were monitored (Figure S29). In particular, carbon capture from various point sources requires a large volume of gases processed (typically 10^6 scfm, standard cubic feet per minute);[30] therefore, the fluid contactor with a lower pressure drop would greatly reduce the process cost. Since the density of Mg_2(dobpdc) was 6 times lower than that of the MgO (~580 and ~3600 kg/m^3, respectively),[31] the final MOF fibers grew in size. As seen in Figures S28 and S29, the pressure drops increased as the number of loaded precursor fibers increased due to the reduced void fraction in the MOF converted module. For example, when more than 12 fibers were loaded into a 1/4" module with a cross-sectional area of 1.17×10^{-5} m^2, deformation of the MOF fiber sorbent occurred during synthesis among adjacent fibers (Figures S29d and S30). The rapid increase in the pressure drop (Figure S28) was observed due to the lowest void fraction of 31% in the module. The module fabricated with nine precursor fibers showed the lowest CO_2 breakthrough capacity (Figure S29a) because sorbate bypassing occurred due to the large void fraction of 49%. As the number of loaded precursor fibers increased up to 11 fibers, it was clear that the void space in the module diminished and the breakthrough capacity increased while the initial pressure drop was retained at increased

https://doi.org/10.1021/jacsau.1c00068
JACS Au 2021, 1, 1198−1207

superficial velocities. Therefore, the module fabricated with 11 precursor fibers (38% void fraction) demonstrated optimal CO_2 sorption performance, which was further tested at different feed conditions for multicycle CO_2 sorption experiments (Figure S31).

Figure 4b–e illustrates the five cyclic sorption–desorption breakthrough profiles of the diamine- and tetraamine-Mg_2(dobpdc)/PEI module with 38% void fraction (i.e., 11 fibers) for different flue gas conditions. Diamine-Mg_2(dobpdc)/PEI showed impressive breakthrough capacity under a dry flue gas flow (Figure 4b), showing the highest uptake in the first cycle of 3.58 mmol/g fiber, and then stabilized at about 3.31 mmol/g fiber after three cycles (8% reduction at the fifth cycle). There was a slight loss in the breakthrough capacity over several thermal cycles because of the partial volatilization of the diamine functional group with low molecular weight.[32] To further simulate realistic feed conditions, cyclic sorption was performed with the humid flue gas (Figure 4d and see Supporting Information for detailed humidification methods). For every humid breakthrough campaign, a prehumidification step was used to reflect realistic conditions. The humid breakthrough capacity of the diamine-Mg_2(dobpdc)/PEI was increased to 4.41 mmol/g fiber due to the formation of bicarbonate species under the presence of water, which increased amine efficiency.[33] However, after the first round of the humidity experiment, a 7% reduction in breakthrough capacity was observed due to the sharpening of the breakthrough curve.

The humid breakthrough capacity was stabilized after three cycles to 3.8 mmol/g fiber (14% reduction in the fifth cycle). The relatively large loss in the sorption capacity of the diamine-Mg_2(dobpdc)/PEI might be due to the high regeneration condition of 120 degrees (Table S3).

A multicyclic sorption test of tetraamine-Mg_2(dobpdc)/PEI was performed under the same conditions. The breakthrough capacities of the tetraamine-Mg_2(dobpdc)/PEI in the first cycle were 2.49 and 4.12 mmol/g fiber in dry and humid conditions (Figure 4c and e), respectively, with the result that the breakthrough CO_2 capacities of the tetraamine-Mg_2(dobpdc)/PEI in flue gas composition were lower than those of diamine. Moreover, the equilibrium time of the tetraamine-Mg_2(dobpdc)/PEI was longer than that of the diamine because the tetraamine, which is bulkier than diamine, caused steric hindrance between neighboring ammonium carbamate chains formed in the CO_2 adsorption.[14] However, the strong interaction between metal-tetraamine or adjacent to the amines maintained humid breakthrough capacity up to 92% after five cycles (Figure 4e). Since the humid feed stream desorbed during regeneration suppresses urea formation, the humid cyclic stability of tetraamine-Mg_2(dobpdc)/PEI was better than dry cyclic stability.[34] In addition, long-term cyclic (up to 200 cycles) stabilities of diamine-/tetraamine-Mg_2(dobpdc)/PEI in humid flue gas composition were measured (Figure 5). Diamine-Mg_2(dobpdc)/PEI showed up to 17% loss in the sorption capacity after 200 cycles and tetreaamine-Mg_2(dobpdc)/PEI showed only 9% loss in the sorption capacity after 200 cycles of continued sorption-desorption of humid flue gas stream. These results support the excellent cyclic stability of the MOF fiber sorbents in modular devices.

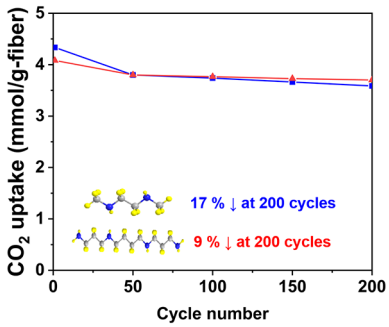

Figure 5. Long-term cyclic stabilities of diamine-/tetraamine-Mg_2(dobpdc)/PEI in flue gas composition at humid conditions (adsorption: 15% CO_2, 15% He, RH 100%, in N_2 balance at 35 °C under 30 sccm for 15 min; desorption: Ar at 120 °C for 30 min).

2.4. CO_2 Sorption at Direct Air Compositions

For negative emission strategies in CCS, the direct air capture (DAC) of CO_2 could reduce the net atmospheric greenhouse gas concentration, providing that economical and energy-efficient devices can be developed and deployed on a large scale. With our "process-ready" module packed with diamine- and tetraamine-Mg_2(dobpdc)/PEI, we further tested the carbon capture performance of these modules in DAC conditions (Figure 6). The multistep CO_2 isotherm of amine-appended Mg_2(dobpdc) affects the sorbate transport during breakthrough measurement, which is more pronounced under ultradilute concentrations in DAC conditions (i.e., 400 ppm of CO_2) than flue gas concentrations.[35] In the breakthrough curves, a shock wave occurs when the slope of the isotherm is steep, whereas a dispersive wave occurs when the slope is gradual.[35] The amine-appended Mg_2(dobpdc)/PEI shows the multiple shock waves consisting of the shock and dispersive waves.[35] The overall breakthrough time in which the CO_2 concentration fell less than 5% of its inlet concentration, and the final equilibrium time was much longer than those of the flue gas case because the mass transfer rate of the amine-functionalized MOF fiber sorbent was reduced by cooperative insertion of CO_2 at lower concentrations.[35] Diamine- and tetraamine-Mg_2(dobpdc)/PEI exhibited dry breakthrough DAC capacities of 0.70 and 1.99 mmol/g fiber, respectively, at 35 °C with 400 ppm of CO_2 (Figure 6).

The diamine-Mg_2(dobpdc)/PEI showed a dual shock wave curve, whereas the tetraamine-Mg_2(dobpdc)/PEI had an extra shock wave at 7.5 h, which is thought to be related to the two-step ammonium carbamate pathway of tetraamine. In addition, since the sorption time was exceptionally long in the tetraamine-Mg_2(dobpdc)/PEI, a flow rate twice as high as that of the diamine case was applied, which not only made the breakthrough profile steeper but also resulted in an increase in dispersive wave concentration. Notably, the tetraamine-Mg_2(dobpdc)/PEI showed an excellent breakthrough CO_2 capacity even at concentrations as low as 400 ppm because the heat of sorption was exceptionally high in the one-step part of the two-step ammonium carbamate chain-reaction mechanism (Figure S23b). Thus, the tetraamine-Mg_2(dobpdc)/PEI with excellent oxidative and thermal stability as well as high heat of sorption was more appropriate than diamine-appended MOF fibers for CO_2 captured from the air. The CO_2 breakthrough capacities of 11 fiber sorbent modules obtained at various operating conditions are summarized in Tables S5 and S6.

https://doi.org/10.1021/jacsau.1c00068
JACS Au 2021, 1, 1198–1207

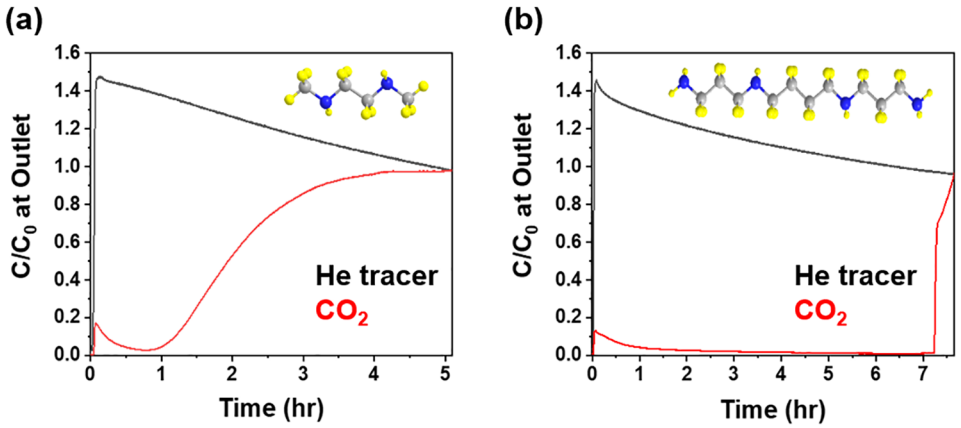

Figure 6. CO_2 sorption at direct air compositions. (a,b) CO_2 breakthrough curves of the (a) diamine-Mg_2(dobpdc)/PEI and (b) tetraamine-Mg_2(dobpdc)/PEI fiber sorbent module (11 fibers) under dry conditions (adsorption: 400 ppm of CO_2, 408 ppm of He, in N_2 balance at 35 °C for 350 min; desorption: Ar at 120 °C for 120 min).

3. CONCLUSIONS

Our results demonstrate that the microporous materials with exceptional CO_2 capacities and stabilities can be solution-processed in a scalable shape (i.e., Type 2 fiber sorbent).[16] Minimized handling steps in the single contactor module approach preserved the original excellent adsorptive properties of the MOF, passing those down to the scaled-up version in fiber shape. It is worth noting that the dry and humid CO_2 capacity of the diamine- and tetraamine-Mg_2(dobpdc)/PEI at flue gas composition have surpassed previously reported cases of fiber sorbents (Table S7).[14,17,23,28,36,37] In our strategy for synthesizing MOFs in the polymeric fiber, recycling of the unreacted ligand or unused solvent through the flow chemistry devices is possible. This approach can greatly reduce the production cost of the MOF-based sorbents. Das et al. has demonstrated a 45% reduction in production cost for MOF-74 with a recycled solvent mixture via a vapor-assisted dry-gel method.[29] In addition, Sinha et al. estimated the energy and cost of mmen-Mg_2(dobpdc) and MIL-101(Cr)-PEI-800 coated monoliths for DAC using the temperature-vacuum swing adsorption (TVSA) process.[38] Both cases showed reasonable carbon capture prices ($60−190 per ton of CO_2 captured). Despite the need for additional studies for the practical application of fiber sorbents, we believe that the flow-synthesized modular fiber sorbent system is a promising platform to demonstrate the cost of less than $100 per ton of CO_2 captured.[38] The current integrative approach shows the opportunities for "lab" to "industry" in the carbon capture field. Our single module approach demonstrated that the designed sorbents, which have different microporosities and diverse functionalities, can be integrated into a rationally designed contactor to advance conventional approaches in CCS as well as uniform reaction of the sorbents in the contactor. These "small footprint" fiber sorbent modules would open the door for the use of the versatile "unspinnable" MOF materials that exhibit tremendous adsorption capacities but have not moved beyond powder-scale experiments.

4. EXPERIMENTAL SECTION

Details of the full materials and experimental methods are explained in the Supporting Information.

4.1. Synthesis of the Amine-Mg_2(dobpdc)/Poly(ether imide) Fiber Sorbents

The synthesis of a 4,4-dihydroxy-(1,1-biphenyl)-3,3-dicarboxylic acid (H_4(dobpdc)) was scaled up based on a previously reported procedure[39] because the ligand is consumed in large amounts in large-scale fiber synthesis. To prevent the destruction of the polymeric matrix by the aprotic solvent during the MOF conversion, the MgO fiber precursors were chemically cross-linked with ethylenediamine and *p*-xylylenediamine solution for 4 h. In the MOF conversion steps, a mass of fiber equivalent to 1.36 mmol of MgO loaded into the polymer matrix is added to 0.25 M ligand solution and reacted at 120 °C for 6 h in a batch reactor or flow module system. The resulting Mg_2(dobpdc)/PEI fiber sorbents were washed with DMF (20 mL × 5) and methanol (20 mL × 5) and activated at 120 °C overnight in a vacuum. Fully activated Mg_2(dobpdc)/PEI fiber sorbents were soaked in diamine solution (containing *N*,*N*′-dimethylethylenediamine: anhydrous hexane) for 4 h or tetraamine solution (*N*,*N*′-bis(3-aminopropyl)-1,4-diaminobutane: anhydrous toluene) for 24 h at 60 °C. The samples were washed with each reaction solvent (3 × 20 mL) and methanol (3 × 20 mL) and dried at 120 °C. The resulting fiber sorbents were activated at 120 °C for 24 h before evaluation of crystallinity, porosity, and CO_2 sorption of the sample.

■ ASSOCIATED CONTENT

Supporting Information

The Supporting Information is available free of charge at https://pubs.acs.org/doi/10.1021/jacsau.1c00068.

Crystallographic data, characterization data (TGA, SEM, EDS, ^{1}H NMR, XRD, cumulative pore volume, N_2 sorption/desorption, pressure drop, and FT-IR) and CO_2 sorption properties (isosteric heat of sorption, CO_2 isotherm, dry/humid CO_2 breakthrough curves, and cyclic stability) of the di/tetraamine-Mg_2(dobpdc)/PEI (PDF)

■ AUTHOR INFORMATION

Corresponding Author

Dong-Yeun Koh − *Department of Chemical and Biomolecular Engineering (BK21 Plus), Korea Advanced Institute of Science and Technology, Daejeon 34141, South Korea; KAIST Institute for NanoCentury, Daejeon 34141, South Korea;* orcid.org/0000-0002-6049-9371; Email: dongyeunkoh@kaist.ac.kr

https://doi.org/10.1021/jacsau.1c00068
JACS Au 2021, 1, 1198−1207

Authors

Young Hun Lee − *Department of Chemical and Biomolecular Engineering (BK21 Plus), Korea Advanced Institute of Science and Technology, Daejeon 34141, South Korea*

YongSung Kwon − *Department of Chemical and Biomolecular Engineering (BK21 Plus), Korea Advanced Institute of Science and Technology, Daejeon 34141, South Korea; Green Carbon Research Center, Korea Research Institute of Chemical Technology, Daejeon 305-600, South Korea*

Chaehoon Kim − *Department of Chemical and Biomolecular Engineering (BK21 Plus), Korea Advanced Institute of Science and Technology, Daejeon 34141, South Korea*

Young-Eun Hwang − *Department of Chemical and Biomolecular Engineering (BK21 Plus), Korea Advanced Institute of Science and Technology, Daejeon 34141, South Korea*

Minkee Choi − *Department of Chemical and Biomolecular Engineering (BK21 Plus), Korea Advanced Institute of Science and Technology, Daejeon 34141, South Korea;* orcid.org/0000-0003-0827-2572

YouIn Park − *Green Carbon Research Center, Korea Research Institute of Chemical Technology, Daejeon 305-600, South Korea*

Aqil Jamal − *Carbon Management Division, Research and Development Center, Dhahran 31311, Saudi Arabia*

Complete contact information is available at: https://pubs.acs.org/10.1021/jacsau.1c00068

Author Contributions

D.-Y.K. conceived the idea and supervised the whole project. Y.H.L. performed the experimental work, and measured the data. D-Y.K., Y.H.L., M.C., and Y.P. wrote the manuscript. Y.K., C.K, and, Y-E.H analyzed and obtained experimental data. A.J. acquired the funding and supervised the project.

Notes

The authors declare no competing financial interest.

■ ACKNOWLEDGMENTS

This research was funded by Saudi Aramco − KAIST CO_2 Management Center. This research was supported by Basic Science Research Program through the National Research Foundation of Korea (NRF) funded by the Ministry of Science, ICT & Future Planning (NRF-2021R1C1C1012014). This work was also supported by the "International Collaborative Energy Technology R&D Program" of the Korea Institute of Energy Technology Evaluation and Planning (KETEP), which was granted financial resources from the Ministry of Trade, Industry & Energy, the Republic of Korea (No. 20188550000580).

■ REFERENCES

(1) Sgouridis, S.; Carbajales-Dale, M.; Csala, D.; Chiesa, M.; Bardi, U. Comparative Net Energy Analysis of Renewable Electricity and Carbon Capture and Storage. *Nat. Energy* **2019**, *4*, 456−465.

(2) Chow, J.; Kopp, R. J.; Portney, P. R. Energy Resources and Global Development. *Science* **2003**, *302*, 1528−1531.

(3) Rochelle, G. T. Amine Scrubbing for CO2 Capture. *Science* **2009**, *325*, 1652−1654.

(4) Sholl, D. S.; Lively, R. P. Seven Chemical Separations to Change the World. *Nature* **2016**, *532*, 435−437.

(5) Khatri, R. A.; Chuang, S. S. C.; Soong, Y.; Gray, M. Carbon Dioxide Capture by Diamine-Grafted SBA-15: A Combined Fourier Transform Infrared and Mass Spectrometry Study. *Ind. Eng. Chem. Res.* **2005**, *44*, 3702−3708.

(6) Fisher, J. C.; Gray, M. Cyclic Stability Testing of Aminated-Silica Solid Sorbent for Post-Combustion CO2 Capture. *ChemSusChem* **2015**, *8*, 452−455.

(7) Choi, W.; Min, K.; Kim, C.; Ko, Y. S.; Jeon, J. W.; Seo, H.; Park, Y. K.; Choi, M. Epoxide-Functionalization of Polyethyleneimine for Synthesis of Stable Carbon Dioxide Adsorbent in Temperature Swing Adsorption. *Nat. Commun.* **2016**, *7*, 1−8.

(8) Peh, S. B.; Zhao, D. Tying Amines down for Stable CO2 capture. *Science* **2020**, *369*, 372−373.

(9) Wang, B.; Côté, A. P.; Furukawa, H.; O'Keeffe, M.; Yaghi, O. M. Colossal Cages in Zeolitic Imidazolate Frameworks as Selective Carbon Dioxide Reservoirs. *Nature* **2008**, *453*, 207−211.

(10) DeWitt, S. J. A.; Sinha, A.; Kalyanaraman, J.; Zhang, F.; Realff, M. J.; Lively, R. P. Critical Comparison of Structured Contactors for Adsorption-Based Gas Separations. *Annu. Rev. Chem. Biomol. Eng.* **2018**, *9*, 129−152.

(11) Zaworotko, M. J. Materials Science: Designer Pores Made Easy. *Nature* **2008**, *451*, 410−411.

(12) Furukawa, H.; Cordova, K. E.; O'Keeffe, M.; Yaghi, O. M. The Chemistry and Applications of Metal-Organic Frameworks. *Science* **2013**, *341*, 1230444.

(13) McDonald, T. M.; Mason, J. A.; Kong, X.; Bloch, E. D.; Gygi, D.; Dani, A.; Crocellà, V.; Giordanino, F.; Odoh, S. O.; Drisdell, W. S.; Vlaisavljevich, B.; Dzubak, A. L.; Poloni, R.; Schnell, S. K.; Planas, N.; Lee, K.; Pascal, T.; Wan, L. F.; Prendergast, D.; Neaton, J. B.; Smit, B.; Kortright, J. B.; Gagliardi, L.; Bordiga, S.; Reimer, J. A.; Long, J. R. Cooperative Insertion of CO2 in Diamine-Appended Metal-Organic Frameworks. *Nature* **2015**, *519*, 303−308.

(14) Kim, E. J.; Siegelman, R. L.; Jiang, H. Z. H.; Forse, A. C.; Lee, J. H.; Martell, J. D.; Milner, P. J.; Falkowski, J. M.; Neaton, J. B.; Reimer, J. A.; Weston, S. C.; Long, J. R. Cooperative Carbon Capture and Steam Regeneration with Tetraamine-Appended Metal-Organic Frameworks. *Science* **2020**, *369*, 392−396.

(15) Reed, D. A.; Keitz, B. K.; Oktawiec, J.; Mason, J. A.; Runcevski, T.; Xiao, D. J.; Darago, L. E.; Crocellà, V.; Bordiga, S.; Long, J. R. A Spin Transition Mechanism for Cooperative Adsorption in Metal-Organic Frameworks. *Nature* **2017**, *550*, 96−100.

(16) Lee, Y. H.; Jeong, J.; Kim, K.; Hyun, T.; Jamal, A.; Koh, D.-Y. Microporous Materials in Scalable Shapes: Fiber Sorbents. *Chem. Mater.* **2020**, *32*, 7081−7104.

(17) Sujan, A. R.; Pang, S. H.; Zhu, G.; Jones, C. W.; Lively, R. P. Direct CO2 Capture from Air Using Poly(Ethylenimine)-Loaded Polymer/Silica Fiber Sorbents. *ACS Sustainable Chem. Eng.* **2019**, *7*, 5264−5273.

(18) Sujan, A. R.; Koh, D. Y.; Zhu, G.; Babu, V. P.; Stephenson, N.; Rosinski, A.; Du, H.; Luo, Y.; Koros, W. J.; Lively, R. P. High-Temperature Activation of Zeolite-Loaded Fiber Sorbents. *Ind. Eng. Chem. Res.* **2018**, *57*, 11757−11766.

(19) Labreche, Y.; Lively, R. P.; Rezaei, F.; Chen, G.; Jones, C. W.; Koros, W. J. Post-Spinning Infusion of Poly(Ethyleneimine) into Polymer/Silica Hollow Fiber Sorbents for Carbon Dioxide Capture. *Chem. Eng. J.* **2013**, *221*, 166−175.

(20) Darunte, L. A.; Terada, Y.; Murdock, C. R.; Walton, K. S.; Sholl, D. S.; Jones, C. W. Monolith-Supported Amine-Functionalized Mg2(Dobpdc) Adsorbents for CO2 Capture. *ACS Appl. Mater. Interfaces* **2017**, *9*, 17042−17050.

(21) Labreche, Y.; Fan, Y.; Rezaei, F.; Lively, R. P.; Jones, C. W.; Koros, W. J. Poly(Amide-Imide)/Silica Supported PEI Hollow Fiber Sorbents for Postcombustion CO2 Capture by RTSA. *ACS Appl. Mater. Interfaces* **2014**, *6*, 19336−19346.

(22) Shakarova, D.; Ojuva, A.; Bergström, L.; Akhtar, F. Methylcellulose-Directed Synthesis of Nanocrystalline Zeolite NaA with High CO2 Uptake. *Materials* **2014**, *7*, 5507−5519.

(23) Lively, R. P.; Leta, D. P.; DeRites, B. A.; Chance, R. R.; Koros, W. J. Hollow Fiber Adsorbents for CO2 Capture: Kinetic Sorption Performance. *Chem. Eng. J.* **2011**, *171*, 801−810.
(24) Li, H.; Eddaoudi, M.; O'Keeffe, M.; Yaghi, O. M. Design and Synthesis of an Exceptionally Stable and Highly Porous Metal-Organic Framework. *Nature* **1999**, *402*, 276−279.
(25) Nemade, K. R.; Waghuley, S. A. Synthesis of MgO Nanoparticles by Solvent Mixed Spray Pyrolysis Technique for Optical Investigation. *Int. J. Met.* **2014**, *2014*, 1−4.
(26) Meckler, S. M.; Li, C.; Queen, W. L.; Williams, T. E.; Long, J. R.; Buonsanti, R.; Milliron, D. J.; Helms, B. A. Sub-Micron Polymer-Zeolitic Imidazolate Framework Layered Hybrids via Controlled Chemical Transformation of Naked ZnO Nanocrystal Films. *Chem. Mater.* **2015**, *27*, 7673−7679.
(27) Xi, G.; Xiong, K.; Zhao, Q.; Zhang, R.; Zhang, H.; Qian, Y. Nucleation-Dissolution-Recrystallization: A New Growth Mechanism for t-Selenium Nanotubes. *Cryst. Growth Des.* **2006**, *6*, 577−582.
(28) Pimentel, B. R.; Fultz, A. W.; Presnell, K. V.; Lively, R. P. Synthesis of Water-Sensitive Metal-Organic Frameworks within Fiber Sorbent Modules. *Ind. Eng. Chem. Res.* **2017**, *56*, 5070−5077.
(29) Das, A. K.; Vemuri, R. S.; Kutnyakov, I.; McGrail, B. P.; Motkuri, R. K. An Efficient Synthesis Strategy for Metal-Organic Frameworks: Dry-Gel Synthesis of MOF-74 Framework with High Yield and Improved Performance. *Sci. Rep.* **2016**, *6*, 1−7.
(30) *How much carbon dioxide is produced per kilowatt hour of U.S. electricity generation?* U.S. Energy Information Administration, Washington, DC. https://www.eia.gov/tools/faqs/faq.php?id=74&=11.
(31) McDonald, T. M.; Lee, W. R.; Mason, J. A.; Wiers, B. M.; Hong, C. S.; Long, J. R. Capture of Carbon Dioxide from Air and Flue Gas in the Alkylamine-Appended Metal-Organic Framework Mmen-Mg 2(Dobpdc). *J. Am. Chem. Soc.* **2012**, *134*, 7056−7065.
(32) Heydari-Gorji, A.; Sayari, A. Thermal, Oxidative, and CO2-Induced Degradation of Supported Polyethylenimine Adsorbents. *Ind. Eng. Chem. Res.* **2012**, *51*, 6887−6894.
(33) Flaig, R. W.; Osborn Popp, T. M.; Fracaroli, A. M.; Kapustin, E. A.; Kalmutzki, M. J.; Altamimi, R. M.; Fathieh, F.; Reimer, J. A.; Yaghi, O. M. The Chemistry of CO2 Capture in an Amine-Functionalized Metal-Organic Framework under Dry and Humid Conditions. *J. Am. Chem. Soc.* **2017**, *139*, 12125−12128.
(34) Jahandar Lashaki, M.; Khiavi, S.; Sayari, A. Stability of Amine-Functionalized CO2 Adsorbents: A Multifaceted Puzzle. *Chem. Soc. Rev.* **2019**, *48*, 3320−3405.
(35) Darunte, L. A.; Sen, T.; Bhawanani, C.; Walton, K. S.; Sholl, D. S.; Realff, M. J.; Jones, C. W. Moving beyond Adsorption Capacity in Design of Adsorbents for CO 2 Capture from Ultradilute Feeds: Kinetics of CO 2 Adsorption in Materials with Stepped Isotherms. *Ind. Eng. Chem. Res.* **2019**, *58*, 366−377.
(36) Lively, R. P.; Chance, R. R.; Kelley, B. T.; Deckman, H. W.; Drese, J. H.; Jones, C. W.; Koros, W. J. Hollow Fiber Adsorbents for CO 2 Removal from Flue Gas. *Ind. Eng. Chem. Res.* **2009**, *48*, 7314−7324.
(37) Li, F. S.; Labreche, Y.; Lively, R. P.; Lee, J. S.; Jones, C. W.; Koros, W. J. Poly(Ethyleneimine) Infused and Functionalized Torlon®- Silica Hollow Fiber Sorbents for Post-Combustion CO2 Capture. *Polymer* **2014**, *55*, 1341−1346.
(38) Sinha, A.; Darunte, L. A.; Jones, C. W.; Realff, M. J.; Kawajiri, Y. Systems Design and Economic Analysis of Direct Air Capture of CO2 through Temperature Vacuum Swing Adsorption Using MIL-101(Cr)-PEI-800 and Mmen-Mg2(Dobpdc) MOF Adsorbents. *Ind. Eng. Chem. Res.* **2017**, *56*, 750−764.
(39) Maserati, L.; Meckler, S. M.; Li, C.; Helms, B. A. Minute-MOFs: Ultrafast Synthesis of M2(Dobpdc) Metal-Organic Frameworks from Divalent Metal Oxide Colloidal Nanocrystals. *Chem. Mater.* **2016**, *28*, 1581−1588.

https://doi.org/10.1021/jacsau.1c00068
JACS Au 2021, 1, 1198−1207